FRICTION-INDUCED VIBRATIONS IN AN EXPERIMENTAL DRILL-STRING SYSTEM FOR VARIOUS FRICTION SITUATIONS

N. Mihajlović† N. van de Wouw, M.P.M. Hendriks, H. Nijmeijer
Eindhoven University of Technology,
Department of Mechanical Engineering,
P.O. Box 513, 5600 MB Eindhoven,
The Netherlands,
N.Mihajlovic@tue.nl, N.v.d.Wouw@tue.nl, M.P.M.Hendriks@tue.nl, H.Nijmeijer@tue.nl

Abstract

Friction-induced limit cycling deteriorates system performance in a wide variety of mechanical systems. In this paper, we study the way in which essential friction characteristics affect the occurrence and nature of friction-induced limit cycling in flexible rotor systems. This study is performed on the level of both numerical and experimental bifurcation analysis. Hereto, an experimental drill-string set-up is used. The synthesis of these numerical and experimental results confirms that friction-induced limit cycling is due to a subtle balance between negative damping at lower velocities and viscous friction at higher velocities. Furthermore, we also show that the level of positive damping in the friction at very small velocities in relation to the level of negative damping appearing for slightly higher velocities determines whether torsional vibrations with and/or without stick-slip can appear. Finally, it is shown how these essential friction characteristics depend on physical conditions such as temperature, normal forces or the type of material in the frictional contact in the experimental set-up.

Key words

Flexible Rotor Systems, Discontinuous Bifurcations, Experimental Non-smooth Dynamics.

1 Introduction

Friction-induced limit cycling often limits the performance and can also endanger the safety of operation of a wide range of mechanical systems. In this paper, we focus on friction-induced limit cycling in mechanical systems with friction and flexibilities. In this context, one can think of drilling rigs, printers, pick and place machines, industrial and domestic robots, simple earth-quake models, accurate mirror positioning systems on satellites and many more. In these systems, the combination of friction and flexibility can give rise to limit cycling. This paper aims at revealing the dependency of limit cycling on the friction characteristics through both numerical and experimental studies. In order to perform experimental validation of the results, an experimental drill-string system is built in which both flexibility and friction are present. This experimental set-up will support the study of friction-induced limit-cycling in general mechanical systems with friction and flexibilities and the study of friction-induced limit-cycling in drill-string systems in particular. The particular interest for drill-string systems is motivated by the presence of unwanted vibration in oil-drilling rigs.

Namely, for the exploration and production of oil and gas, deep wells are drilled with a rotary drilling system. A rotary drilling system creates a borehole by means of a rock-cutting tool, called a bit. The torque driving the bit is generated at the surface by a motor with a mechanical transmission box. Via the transmission, the motor drives the rotary table: a large disc that acts as a kinetic energy storage unit. The medium to transport the energy from the surface to the bit is a drill-string, mainly consisting of drill pipes. The lowest part of the drill-string is the Bottom-Hole-Assembly consisting of drill collars and the bit. The drill-string undergoes various types of vibrations during drilling: torsional (rotational) vibrations caused by interaction between the bit and well, bending (lateral) vibrations caused by pipe eccentricity, axial (longitudinal) vibrations due to bouncing of the bit and hydraulic vibrations in the circulation system, stemming from pump pulsations. Drill-string vibrations are an important cause for premature failure of drill-string components and drilling inefficiency. In this paper, only torsional drill-string vibrations are investigated. Drill rigs should generally operate at constant down-hole velocities (realized by a

†Current address: Philips Research Laboratories,
Prof. Holstlaan 4, 5656 AA Eindhoven, The Netherlands,
e-mail: Nenad.Mihajlovic@philips.com

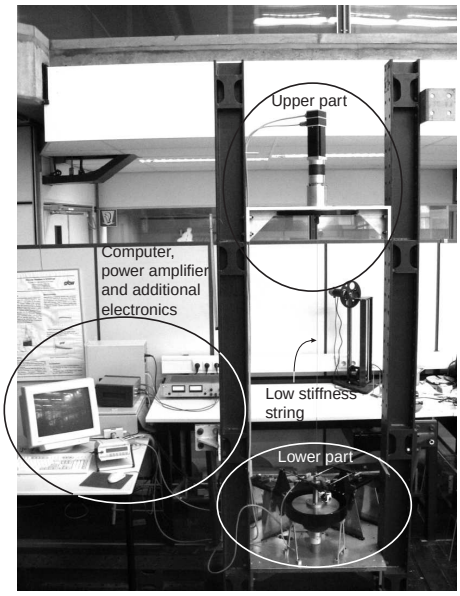

Figure 1. Experimental drill-string set-up.

constant torque at the rotary table); therefore, the focus of this investigation is on the steady-state behavior of drill-string systems.

Extensive research on the subject of torsional vibrations has already been conducted (Cunningham, 1968; Brett, 1992; Jansen and van den Steen, 1995; Kreuzer and Kust, 1996; Leine *et al.*, 2002). The cause for torsional vibrations is the stick-slip phenomenon due to the friction force between the bit and the well c.f. (Jansen and van den Steen, 1995; Leine *et al.*, 2002). Moreover, the cause for the torsional vibrations is negative damping in the friction force present due to the contact between the bit and the borehole c.f. (Brett, 1992; Kreuzer and Kust, 1996). Friction-induced limit cycling is a performance limiting factor in many mechanical systems. Survey papers on friction-induced limit cycling are (Brockley *et al.*, 1967; Ibrahim, 1994a; Ibrahim, 1994b), in which specific friction characteristics are coupled to the existence of such limit cycling. Moreover, in (Popp *et al.*, 2002) causes for friction-induced limit cycling, such as negative damping and fluctuating normal forces, are discussed. However, a limited amount of experimental work on friction-induced limit cycling in non-controlled systems is available (Krauter, 1981; Mihajlović *et al.*, 2004; Mihajlović, 2005; Mihajlović *et al.*, 2005*a*; Mihajlović *et al.*, 2005*b*).

In order to gain improved understanding in the causes for torsional vibrations, an experimental drill-string set-up is built, see figure 1. This experimental set-up consists of two discs, connected by a string. The upper disc is driven by a motor and at the lower disc a brake is implemented to exert a friction force on the disc. In this paper, we investigate along several routes how the occurrence and nature of the friction-induced vibrations depend on specific friction characteristics. Firstly, an extensive numerical bifurcation analysis is performed for changing friction characteristics. Secondly, such bifurcation analysis is also performed on an experimental level to confirm the validity of the model-based results. Furthermore, physical conditions, such as temperature and the normal force applied to the brake, are changed in the experiments to illuminate the influence of such changes on the friction and on the vibrations induced by the friction. Moreover, we compare the results obtained with the set-up shown in figure 1 with the results obtained in (Mihajlović *et al.*, 2004; Mihajlović *et al.*, 2005*a*), since in (Mihajlović *et al.*, 2004; Mihajlović *et al.*, 2005*a*) torsional vibrations are obtained as a result of other brake material. The numerical and experimental results jointly constitute a clear and coherent view on the way in which friction-induced limit cycles arise and change under changing frictional conditions.

In the next section, the experimental set-up is introduced. Subsequently, the model of the set-up and the estimates for its parameters are discussed. Next, the dependency of the friction-induced limit cycling on specific friction characteristics is studied on a model level by means of an extensive numerical bifurcation analysis. The model-based results are compared to experimental results and the dependency of the occurrence of torsional vibrations on certain physical frictional conditions is investigated on an experimental level. Finally, a discussion of the obtained results and concluding remarks are presented.

2 The Experimental Set-Up

The experimental drill-string set-up is shown in figure 1. The set-up consists of a power amplifier, a DC-motor, two rotational (upper and lower) discs, a low-stiffness string and an additional brake applied to the lower disc. The input voltage from the computer is fed into the DC-motor via the power amplifier. The DC-motor is connected to the upper steel disc via the gear box, see figure 2. The upper disc and the lower disc are connected through a low stiffness steel string. Both discs can rotate around their respective geometric centers and the related angular positions are measured using incremental encoders (see figure 2 for the encoder at the upper disc).

A brake and a small oil-box with felt stripes are fixed to the upper bearing housing of the lower part of the set-up, see figure 3. With the brake, a range of normal forces can be applied and the contact between the brake

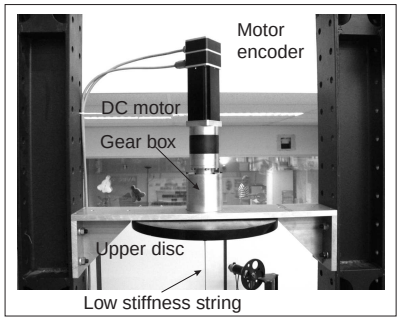

Figure 2. The upper part of the experimental drill-string set-up.

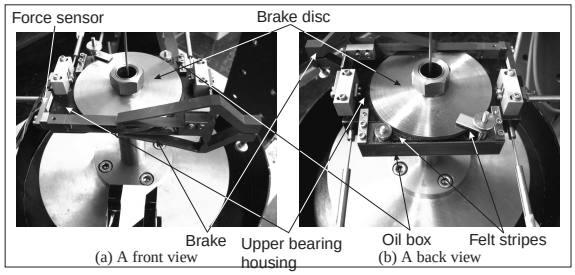

Figure 3. The lower part of the set-up.

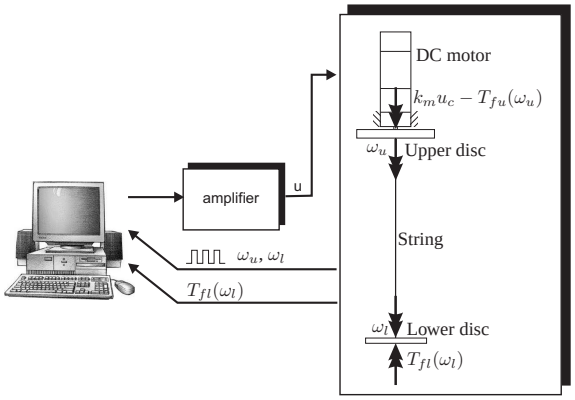

Figure 4. Schematic representation of the drill-string set-up.

and the brake disc produces a friction force exerted on the brake disc. This friction force can induce torsional vibrations in the set-up. The brake contact material is bronze. The steel brake disc is connected to the lower brass disc via a very stiff shaft. The oil-box with the felt stripes is constructed in order to add oil (ondina oil 68) to the brake disc in a reproducible way. This oil lubrication will prove to be crucial for the existence of torsional vibrations in the set-up.

3 Model of the Set-Up

In this section, we introduce a dynamic model of the experimental drill-string set-up which is used throughout the paper. The system is depicted schematically in figure 4.

By θ_u and θ_l we denote the angular displacements of the upper and lower disc, respectively. Moreover, $\omega_u = \dot{\theta}_u$ and $\omega_l = \dot{\theta}_l$ represent the angular velocities of the upper and lower disc, respectively. Furthermore, $\alpha = \theta_l - \theta_u$ is the relative angular displacement of the lower disc with respect to the upper disc. In the sequel, we will use the state vector $\mathbf{x}$ defined by $\mathbf{x} = \left[\alpha\ \omega_u\ \dot{\alpha}\right]^T$. The equations of motion of the system are given by:

$$\begin{aligned} J_u\dot{\omega}_u - k_\theta\alpha + T_{fu}(\omega_u) &= k_m u, \\ J_l(\ddot{\alpha} + \dot{\omega}_u) + T_{fl}(\omega_u + \dot{\alpha}) + k_\theta\,\alpha &= 0, \end{aligned} \tag{1}$$

where J_u and J_l are the moments of inertia of the upper and lower discs about their respective centers of mass, k_θ is the torsional spring stiffness and k_m is the motor constant. It should be noted that the friction torque at the upper disc $T_{fu}(\omega_u)$ is due to friction in the bearings of the upper disc and due to the electro-magnetic effect in the DC-motor, and the friction torque at the lower disc $T_{fl}(\omega_l)$ comprises the friction in the bearings of the lower disc and the friction induced by the brake-mechanism. Both friction torques are modeled using set-valued force laws:

$$\begin{aligned} T_{fu}(\omega_u) &\in \begin{cases} T_{cu}(\omega_u)\mathrm{sgn}(\omega_u) & \text{for } \omega_u \neq 0, \\ [-T_{cu}(0^-),\, T_{cu}(0^+)] & \text{for } \omega_u = 0, \end{cases} \\ T_{fl}(\omega_l) &\in \begin{cases} T_{cl}(\omega_l)\mathrm{sgn}(\omega_l) & \text{for } \omega_l \neq 0, \\ [-T_{cl}(0^-),\, T_{cl}(0^+)] & \text{for } \omega_l = 0, \end{cases} \end{aligned} \tag{2}$$

where the velocity dependency of the friction at the upper disc is expressed through $T_{cu}(\omega_u)$, with

$$T_{cu}(\omega_u) = T_{su} + \triangle T_{su}\mathrm{sgn}(\omega_u) + b_u|\omega_u| + \triangle b_u\omega_u, \tag{3}$$

and the velocity dependency of the friction at the lower disc is expressed through $T_{cl}(\omega_u)$, consisting of a Stribeck model with viscous friction:

$$T_{cl}(\omega_l) = T_{cl} + (T_{sl} - T_{cl})e^{-|\omega_l/\omega_{sl}|^{\delta_{sl}}} + b_l|\omega_l|. \tag{4}$$

Equation (3) expresses the fact that we model the friction at the upper disc as a combination of static friction and viscous friction and that it is asymmetric. Herein, $T_{cu}(0^+) = T_{su} + \triangle T_{su}$ and $-T_{cu}(0^-) = -T_{su} + \triangle T_{su}$ represent the maximum and minimum value of the friction torque for zero angular velocities and $b_u + \triangle b_u$ and $b_u - \triangle b_u$ are viscous friction coefficients for positive and negative velocities, respectively. In (4), T_{cl} and T_{sl} represent the Coulomb friction and static friction levels, respectively, ω_{sl} is the Stribeck velocity, δ_{sl} the Stribeck shape parameter and b_l the viscous friction coefficient.

The parameters of the model are estimated using a nonlinear least-squares technique. Hereto, persistently exciting input voltage signals are taken as inputs for the experimental system and the angular positions of both discs are measured. Next, the response of the model to such inputs is simulated and an optimal set of parameter estimates is calculated based on matching the measurements and simulations in a least-squares sense. For more detailed information on the identification procedure and the validation results we refer to (Mihajlović *et al.*, 2004; Mihajlović, 2005). Here, we summarize the result of this extensive identification procedure in Table 1. In the remainder of this paper this parameter set will be referred to as the 'nominal' set of parameters. Especially the friction situation at the lower disc is varied, with respect to this nominal situation, in order to investigate its influence on the friction-induced limit-cycling. Figure 5 shows the identified friction models, which indicates a pronounced Stribeck effect in the friction at the lower disc. It should be noted that here a normal force of 20.5 N is applied to the brake. In figure 5, we can recognize different friction regimes as depicted schematically in figure 6, see also (Armstrong-Hélouvry *et al.*, 1994).

Parameter		Estimated value
J_u	[kg m^2/rad]	0.4765
k_m	[Nm/V]	4.3228
T_{su}	[Nm]	0.37975
ΔT_{su}	[Nm]	-0.00575
b_u	[Nms/rad]	2.4245
Δb_u	[Nms/rad]	-0.0084
k_θ	[Nm/rad]	0.0775
J_l	[kg m^2/rad]	0.0414
T_{sl}	[Nm]	0.2781
T_{cl}	[Nm]	0.0473
ω_{sl}	[rad/s]	1.4302
δ_{sl}	[-]	2.0575
b_l	[Nms/rad]	0.0105

Table 1. Parameter estimates.

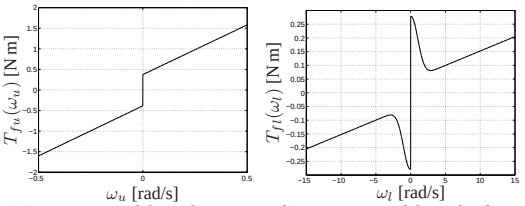

(a) Friction model at the upper disc. (b) Friction model at the lower disc.

Figure 5. Estimated friction models.

4 Steady-State Analysis of the Dynamics

In this section, we study the steady-state behavior of the drill-string system for constant values of the input voltage $u = u_c$ on a model level. Such steady-state behavior is of particular interest in drill-string systems since these types of systems are generally driven by a constant torque while aiming at a constant velocity at the lower part of the set-up. Such constant-velocity condition reflects equilibria of (1). These equilibria involve isolated equilibria (in which $\omega_u = \omega_l \neq 0$) and equilibrium sets (in which $\omega_u = \omega_l = 0$). In such an equilibrium set the deformation of the drill-string α can attain values in a set due to the set-valued nature of the friction force laws. For analytical expressions for these equilibria and both local and global (Lyapunov-based) stability analysis of the equilibria, see (Mihajlović, 2005; Mihajlović *et al.*, 2005*b*). Firstly, the bifurcation diagram with the constant input voltage as a bifurcation parameter is presented for the nominal friction model at the lower disc, as introduced in figure 5(b). Secondly, the dependency of the steady-state behavior on the friction characteristics at the lower disc is investigated.

4.1 Bifurcation Diagram (Nominal Case)

Here we analyze the steady-state behavior (equilibria and limit cycles) of the estimated model, with parameters as in Table 1. More specifically, a bifurcation diagram with u_c as a bifurcation parameter is constructed. In this bifurcation diagram, branches of equilibria and branches of limit cycles are depicted. Using a path following technique in combination with a shooting method (Ascher *et al.*, 1995; Parker and Chua, 1989),

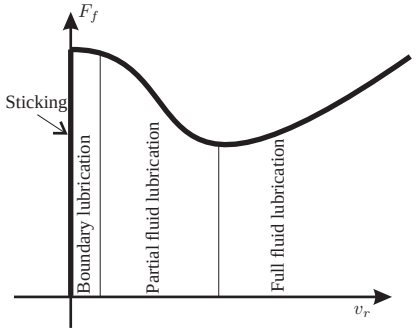

Figure 6. Different regimes in the friction force.

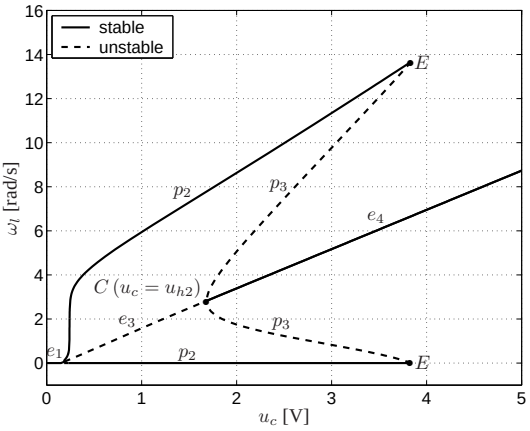

(a) The bifurcation diagram.

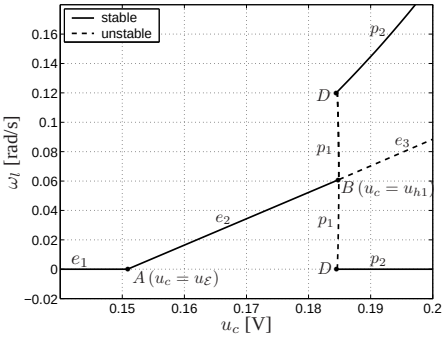

(b) Bifurcation diagram for small input voltages.

Figure 7. Bifurcation diagram of system (1) with parameters as in table 1.

these limit cycles are computed numerically. Herein, the so-called switch model (Leine and Nijmeijer, 2004) is used to properly deal with the discontinuities in the dynamics, related to the set-valued nature of the friction models.

The results of an extensive bifurcation analysis are shown in bifurcation diagram in figure 7, with u_c as a bifurcation parameter. In those figures, the maximal and minimal values of ω_l are plotted when a limit cycle is found. Floquet multipliers, corresponding to these limit cycles, are computed numerically and used to determine the local stability properties of these limit cycles. With respect to the obtained results, the following remarks can be made.

For $u_c < u_\mathcal{E}$, an equilibrium set exists, indicated by

branch e_1, which condenses to an equilibrium point at point A and progresses as an equilibrium branch e_2 of isolated equilibria. Point B ($u_c = u_{h1}$) represents a subcritical Hopf bifurcation point. For $u_c > u_{h1}$ an unstable equilibrium branch e_3 exists and from point B an unstable periodic branch p_1 consisting of limit cycles without stick-slip arises, see figure 7(b). The unstable periodic branch p_1 is connected to a locally stable periodic branch p_2 at the point D, which represents a fold bifurcation point. Since the periodic branch p_2 consists of limit cycles which represent torsional vibrations with stick-slip, point D represents a discontinuous fold bifurcation. Periodic branch p_2 consists only of locally stable limit-cycles with stick-slip, due to the non-smooth nonlinearities in the friction torque at the lower disc. For some higher constant input voltage u_c (point E in figure 7(a)) the locally stable periodic branch p_2 disappears through another discontinuous fold bifurcation. At this fold bifurcation point, the stable periodic branch p_2 merges with an unstable periodic branch p_3. The unstable periodic branch p_3 is connected to the equilibrium branches e_3 and e_4 in the subcritical Hopf bifurcation point C ($u_c = u_{h2}$).

In (Mihajlović, 2005; Mihajlović *et al.*, 2005*b*), on the basis of a theoretical stability analysis it is concluded that the presence of negative damping in the friction at the lower disc induces the Hopf bifurcation point B leading to limit cycling. More specifically, a local stability condition for the isolated equilibria (e_2, e_3 and e_4) can be formulated by:

$$\left.\frac{\mathrm{d}T_{cl}}{\mathrm{d}\omega_l}\right|_{\omega_l=\omega_{eq}} > d, \tag{5}$$

where ω_{eq} is the value of ω_l in equilibrium and d is given by

$$d = \frac{-J_u^2 k_\theta - (b_u+\triangle b_u)^2 J_l}{2\,J_u(b_u+\triangle b_u)} + \frac{\sqrt{(J_u^2 k_\theta + (b_u+\triangle b_u)^2 J_l)^2 - 4\,J_u J_l^2 k_\theta (b_u+\triangle b_u)^2}}{2\,J_u(b_u+\triangle b_u)}. \tag{6}$$

Note that for the friction model in figure 5(b), this condition is not satisfied for branch e_3, so for equilibrium values of the angular velocity of the lower disc in the set $[0.0610, 2.830]$ rad/s. Clearly, the second Hopf bifurcation point C occurs when ω_{eq} is approximately at the minimum of $T_{fl}(\omega_l)$ (for $\omega_l > 0$), i.e. when the viscous friction starts to dominate over negative damping effects.

So, the range (in terms of u_c) for which limit cycling occurs is limited by the presence of viscous damping at higher angular velocities. Moreover, there exists a range of input voltages for which both stable equilibria and stable limit cycles exist. This co-existence can be explained by the fact that the viscous friction is only dominant in a neighborhood (in state-space) of the equilibria and outside this neighborhood the negative damping effect comes into play once more giving rise to limit cycling. On this limit cycle a steady-state balance between the 'stabilizing' effect of viscous friction (at higher velocities) and the 'destabilizing' effect of negative damping (at lower velocities) is attained. The magnitude of the range of angular velocities is determined by a balance between the level of negative damping and viscous damping. The fact that such subtle balance between negative damping and viscous friction is a crucial factor in the qualitative steady-state behavior will be confirmed in the next section, in which the dependency of this behavior on these friction characteristics is studied.

4.2 Changes in the Friction Characteristics

The previous section shows that the friction characteristics largely determine whether or not limit cycling occurs. Now, we discuss the influence of these characteristics of the friction at the lower disc on the steady-state behavior of the system. In doing so, we use the friction model in figure 5(b) and the resulting bifurcation diagram, see figure 7, as a reference situation (i.e. the nominal case). The study of the stability of the equilibria in (Mihajlović, 2005; Mihajlović *et al.*, 2005*a*; Mihajlović *et al.*, 2005*b*) shows that these stability properties are closely connected to two specific friction characteristics: firstly, the negative damping/Stribeck-effect and, secondly, the presence of viscous friction at higher velocities. Furthermore, in (Mihajlović, 2005; Mihajlović *et al.*, 2005*a*) it is shown that when the level of positive damping in the friction at very small velocities is high enough in relation to the level of negative damping present at slightly higher velocities, torsional vibrations with and without stick-slip appear. Therefore, in this section we explicitly investigate the influence of these three friction characteristics (positive damping at very low velocities, negative damping at slightly higher velocities and viscous friction) on the steady-state behavior (bifurcation diagram). In order to isolate the influence of these friction characteristics, we first change the friction model only at very low velocities. Next, we change the friction model such that the negative damping changes while the friction characteristics at very low velocities and viscous damping level remain the same. Finally, the friction model is changed such that the viscous damping level changes, while the level of positive damping at very low velocities and the negative damping level remain unchanged.

4.2.1 Changes in the Low-Velocity Characteristics

To analyze the influence of the low-velocity characteristics of $T_{fl}(\omega_l)$ on the steady-state behavior of the set-up (1), we consider various friction situations which differ only for very low angular velocities (however, the static friction level T_{sl} is the same), as shown in figure 8(a). In one friction situation the damping at very low velocities is positive and higher (dark-grey line in figure 8(a)) than the positive damping in the nominal friction model (light-grey line in figure 8(a)) and in the second friction situation the damping at very low velocities is negative (black line in figure 8(a)). For such friction

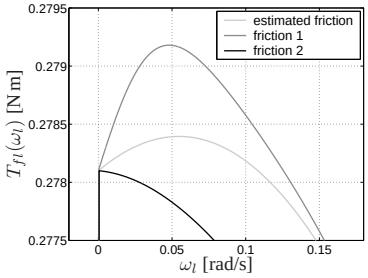

(a) Friction torques for various levels of damping at low angular velocities.

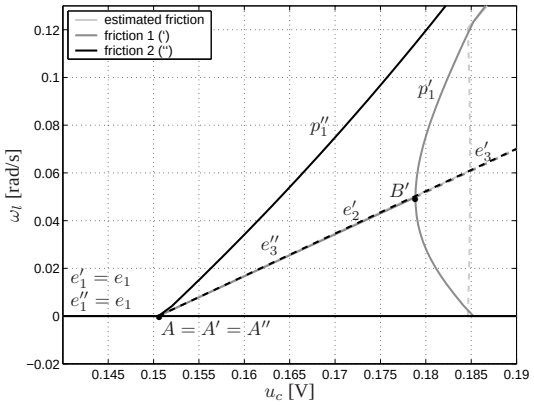

(b) Bifurcation diagrams.

Figure 8. Friction torques for various friction characteristics at very low velocities and related bifurcation diagrams.

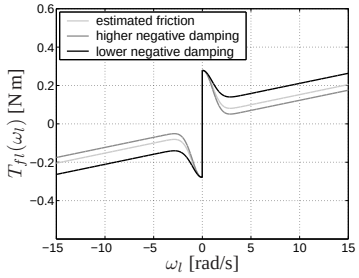

(a) Friction torques for various levels of negative damping.

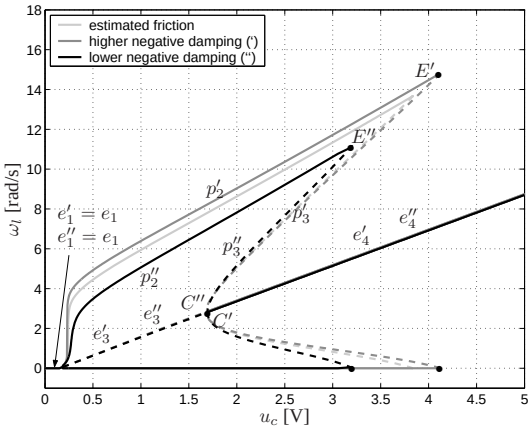

(b) Bifurcation diagrams.

Figure 9. Friction torques for various negative damping and related bifurcation diagrams.

torques, related bifurcation diagrams are constructed. It appears that the obtained bifurcation diagrams differ only for very low velocities, hence we show the related bifurcation diagrams only for low input voltages u_c, see figure 8(b).

When we compare the obtained bifurcation diagrams for low input voltages, the following can be concluded. Firstly, equilibrium branches e_1, e_1' and e_1'' are identical. Secondly, if the friction damping at very low velocities is high enough with respect to the negative damping ('friction 1' in figure 8(b)), then from bifurcation point B' a locally unstable equilibrium branch e_3' and a locally stable periodic branch p_1' arise through a *supercritical* Hopf bifurcation. Since, the periodic branch p_1' consists of limit-cycles which represent torsional vibrations *without* stick-slip, point B' represents a *smooth* supercritical Hopf bifurcation point. However, if the damping at the low velocities is negative enough ('friction 2' in figure 8(b)), torsional vibrations appear immediately when the system leaves the sticking region. Consequently, in point A'' a stable equilibrium branch e_1'', an unstable equilibrium branch e_3'' and a stable periodic branch p_2'' are connected as shown with the black line in figure 8(b). A stable equilibrium branch e_1'' consists of locally stable equilibrium sets (which exist due to sticking phenomenon) and the periodic branch p_1'' consists of limit cycles which represent torsional vibrations with stick-slip. Therefore, point A'' represents a discontinuous bifurcation point. Moreover, such bifurcation point looks like a kind of discontinuous supercritical Hopf bifurcation point described in (Leine and Nijmeijer, 2004). However, since e_1'' consists of equilibrium sets and of equilibrium point A'', and not only of equilibrium points, this is not the case here.

4.2.2 Changes in the Negative Damping In order to analyze the influence of various negative damping levels in $T_{fl}(\omega_l)$ on the steady-state behavior of the drill-string system (1), we consider two friction situations that differ from the nominal case, see figure 9(a). In all cases, both the static friction level T_{sl} and the viscous damping coefficient b_l coincide. The adapted friction models are such that the minimum of the friction curve (for $\omega_l > 0$) occurs at the same angular velocity for all friction models. Consequently, Hopf bifurcation points (B', B'' and C', C'') appear at approximately the same input voltages u_{h1} and u_{h2}, respectively, for all friction models, see figure 9(b). However, in one friction situation the negative damping is higher (dark-grey line in figure 9(a)) and in the second friction situation the negative damping is lower (black line in figure 9(a)) than in the nominal friction model (light-grey line in figure 9(a)). The related bifurcation diagrams are shown in figure 9(b).

When we compare these bifurcation diagrams the following conclusions can be drawn. Firstly, equilibrium branches e_1, e_1' and e_1'' are identical for all friction situations. Secondly, if the negative damping is lower (black line in figure 9(a)), then torsional vibrations disappear for lower constant input voltages (compare dis-

continuous fold bifurcation points E' and E'' in figure 9(b)). In other words, if the negative damping in the friction torque at the lower disc is lower, then torsional vibrations can appear for a smaller range of input voltages u_c. This is due to the fact that the region of coexistence of stable equilibria and stable limit cycles decreases in such a case. Finally, from figure 9(b), we can conclude that a lower negative damping level causes lower amplitudes of the torsional vibrations in the drill-string system. Indeed, a lower negative damping level causes the friction force to be higher (see figure 9(a)), the dissipation of the energy due to such friction is higher, which in turn leads to a lower amplitude of the torsional vibrations.

4.2.3 Changes in the Viscous Friction In order to discuss the influence of various viscous friction levels in $T_{fl}(\omega_l)$ on the steady-state behavior of the drill-string system (1), we consider two friction situations in comparison with the nominal friction torque, see figure 10(a). In all friction situations, the static friction level T_{sl} is the same and the friction torques differ only for high angular velocities ω_l. For small velocities (approximately up to velocities where the friction curve reaches a minimum (for $\omega_l > 0$)) the friction models coincide. As a consequence, the Hopf bifurcation points coincide. In one friction situation, the viscous friction level is higher (dark-grey line in figure 10(a)) and, in the second friction situation, the viscous friction level is lower (black line in the same figure) than in the nominal friction torque (light-grey line). The related bifurcation diagrams are shown in figure 10(b). When we compare the obtained bifurcation diagrams, the following conclusions can be drawn. Firstly, equilibrium branches e_1, e_1' and e_1'' are identical for all friction situations. Secondly, if the viscous friction level is lower, then the fold bifurcation point E'' appears for higher constant input voltages; i.e. in such cases torsional vibrations can appear for a larger range of input voltages u_c (compare discontinuous fold bifurcation points E' and E'' in figure 10(b)). In other words, for a lower viscous damping level torsional vibrations can appear in a larger range of input voltages, due to the fact that the region of coexistence of stable equilibria and stable limit cycles increases. In figure 10(b), we observe that a lower viscous friction level causes higher amplitudes of the torsional vibrations in the system. Namely, when the viscous friction level is lower, then the friction torque is also lower (see figure 10(a)); hence, the dissipated energy is lower and the amplitude of torsional vibrations is higher.

When comparing figures 9(b) and 10(b) we can conclude that a change in negative damping level and a change in the viscous friction level can have a qualitatively similar effect on the friction-induced limit cycling. Therefore, we can conclude that a balance between the negative damping and the viscous friction levels determines the range (in terms of u_c) in which limit cycling occurs. This effect will be illustrated in experiments in the next section.

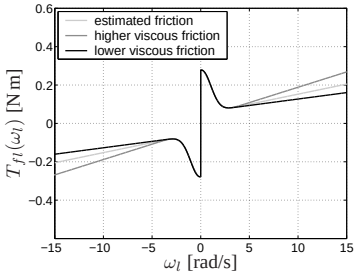

(a) Friction torques for various viscous friction levels.

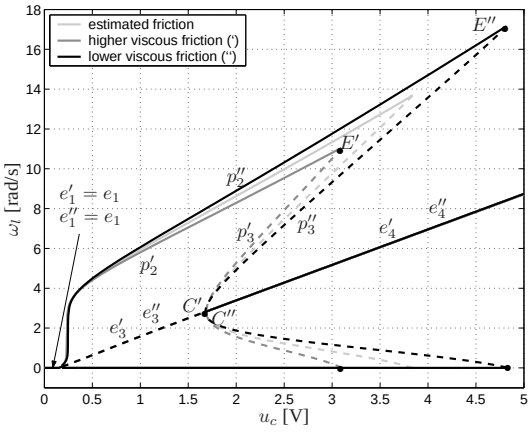

(b) Bifurcation diagrams.

Figure 10. Friction torques for various viscous friction levels and related bifurcation diagrams.

5 Experiments

In this section, the steady-state behavior (for constant input voltages) of the experimental drill-string system is studied and compared to the model-based results. Firstly, the bifurcation diagram of estimated (nominal) case is compared to an experimentally constructed bifurcation diagram. Secondly, in analogy to the previous section, the dependency of the steady-state behavior on the friction characteristics is studied experimentally.

5.1 Bifurcation Diagram (Nominal Case)

In order to check the validity of the obtained model of the drill-string set-up when ondina oil 68 is used as a lubrication fluid and a $20.5\,\mathrm{N}$ normal force is applied at the brake, experimental results are compared with the model-based results. As already mentioned earlier, the predictive quality of the estimated model in steady-state is of great interest. Therefore, when a constant voltage is applied at the input of the set-up, each experiment lasts long enough to guarantee that all transient effects have disappeared and then the last part of the measurement signals is recorded.

The same type of bifurcation diagram, as shown in figure 7, is constructed experimentally. In order to construct such experimental bifurcation diagram, a range of constant input voltages is applied to the set-up. When no torsional vibrations are observed (the system is in equilibrium), the mean value of the recorded angular velocity of the lower disc is computed and the obtained data are plotted using the symbol "**x**". When

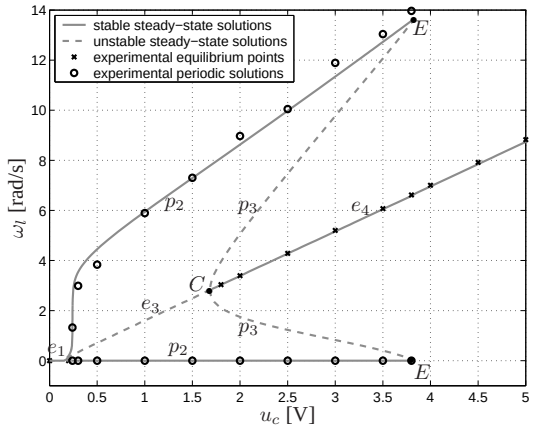

Figure 11. Comparison of the simulated and experimental bifurcation diagram.

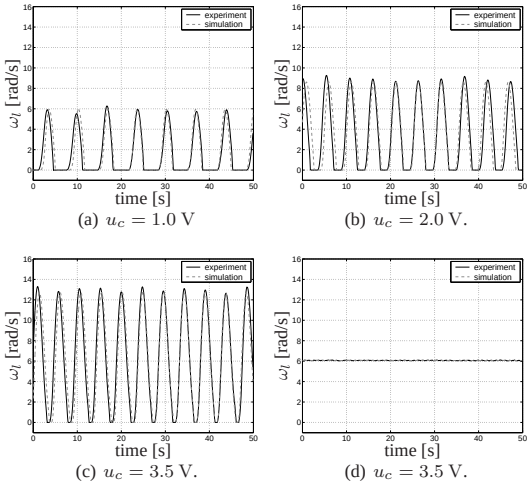

(a) $u_c = 1.0$ V (b) $u_c = 2.0$ V. (c) $u_c = 3.5$ V. (d) $u_c = 3.5$ V.

Figure 12. Experimental and simulated angular velocity at the lower disc for various constant input voltages and various initial conditions.

torsional vibrations are observed at the lower disc, the mean value of local maxima and the mean value of local minima of the vibrations are computed. Then, these experimentally obtained data are plotted using the symbol "**o**". Such experimental results, together with the bifurcation diagram obtained by a numerical analysis of the estimated model, are shown in figure 11.

Both in the numerical and the experimental bifurcation diagram we notice qualitatively different behavior of the system when the constant input voltage is changed. Firstly, for very low input voltages the system has an equilibrium set (i.e. the system is in the sticking phase). Secondly, if the input voltage is increased, the system enters the region where only torsional vibrations (i.e. stable limit cycles) appear. Thirdly, if the input voltage is even higher, then the input voltage is in the region where torsional vibrations (stable limit cycles) and a constant angular velocity at the lower disc (stable equilibrium points) co-exist in the set-up. Finally, if the input voltage is high enough ($u_c > 3.8\,\mathrm{V}$), the system enters the region where no torsional vibrations can appear in the system in steady-state.

In order to show that the experimental behavior indeed matches well with the model behavior, a confrontation between the experimentally and numerically obtained time-series is provided in figure 12. In this figure, the experimental angular velocity (solid black line) and the angular velocity obtained using the estimated model (dashed grey line) in steady-state are shown for different constant input voltages. Namely, the signals presented in figures 12(a), 12(b) and 12(c) represent stick-slip limit-cycling (torsional vibrations) and figure 12(d) represents an equilibrium point. Clearly, the combination of figure 12(c) and figure 12(d) confirms that in the experiments a region exists for which both stable equilibria and stable limit cycles exist. From the comparison between simulation and experimental results, it can be concluded that with the suggested model the steady-state behavior of the set-up is modeled accurately.

5.2 Changes in the Friction Characteristics

We have already analyzed how various changes in the friction characteristics can influence torsional vibrations in drill-string systems on a model level. Here, we investigate the way in which various friction conditions influence torsional vibrations in the experimental set-up.

In the experimental set-up, shown in figure 1, only torsional vibrations with stick-slip occur as a result of a contact between the bronze brake material and the steel brake disc with ondina oil 68 as a lubricant. In (Mihajlović, 2005; Mihajlović *et al.*, 2005*a*) torsional vibrations with and without stick-slip are obtained when a brake, with rubber brake material, is applied to the lower brass disc, with water as a lubricant. Then, for the estimated friction model the damping at the lower velocities is high enough with respect to the following negative damping. Consequently, those results, together with the results presented in Section 4.2.1 (see figure 8), confirm that the combination of a low negative damping in the friction torque together with a high positive damping at a very low velocities is responsible for the appearance of torsional vibrations without stick-slip. Moreover, in (Mihajlović, 2005) it is concluded that such friction characteristics at low velocities are mainly caused by the damping characteristics of the brake material (rubber).

5.2.1 Changes in the Applied Normal Force In order to analyze how changes in the normal force, which is applied to the brake, influence the steady-state behavior of the set-up, we apply a $18\,\mathrm{N}$ and a $12.2\,\mathrm{N}$ normal force to the brake. Next, the parameters of the model of the obtained friction torques are estimated, using the same identification procedure as used to identify the nominal model. The obtained models are validated and numerical and experimental bifurcation diagrams are constructed for both normal force levels. The estimated friction models $T_{fl}(\omega_l)$ are shown in figure 13(a). The related bifurcation diagrams are shown

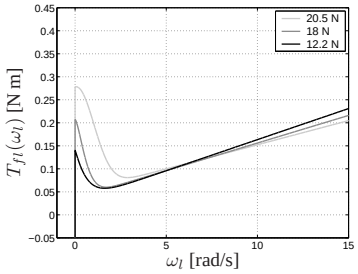

(a) Estimated friction models for the friction at the lower disc for various normal force levels applied at the brake.

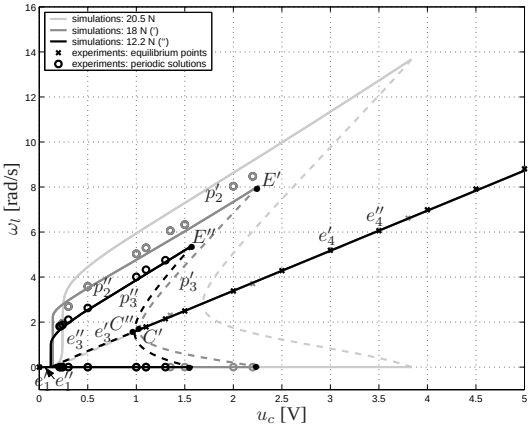

(b) Bifurcation diagrams.

Figure 13. Dependency of the friction characteristics and the bifurcation diagram on various normal force levels applied at the brake.

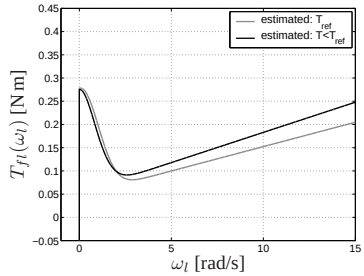

(a) Estimated friction model at the lower disc for various temperatures.

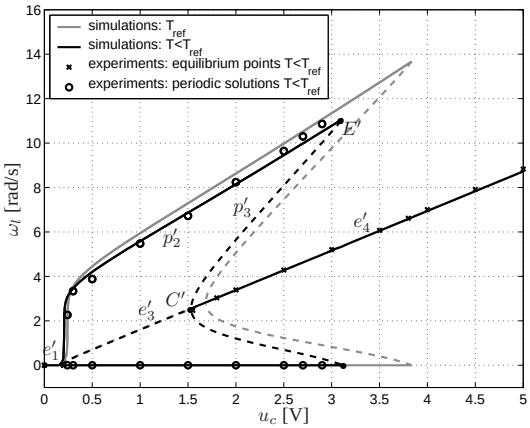

(b) Bifurcation diagrams.

Figure 14. Dependency of the friction characteristics and the bifurcation diagram on temperature changes: $T \in [17°\text{C}, 22°\text{C}]$ and $T_{ref} \in [25°\text{C}, 30°\text{C}]$.

in figure 13(b). Again, the experimental and model-based results correspond well.

When a lower normal force is applied to the brake, the static friction level is lower, the sticking region decreases and the lower disc starts to rotate for lower input voltages. Furthermore, for lower normal force levels, the separation process between the contacting surfaces (brake disc and the brake blocks) and, therefore, the full fluid lubrication regime occur for lower velocities, see figure 6).

As mentioned before, the position of the second Hopf bifurcation point is determined approximately by the point where the friction curve $T_{fl}(\omega_l)$ reaches its minimum (for $\omega_l > 0$). This, in fact, corresponds to the point where full fluid lubrication appears (see figure 6). Consequently, for lower normal force levels, the Hopf bifurcation points C' and C'' in figure 13(b) appear for lower input voltages and the region increases, in which a constant velocity at the lower disc (a stable equilibrium) can appear.

Figure 13(a) indicates that the main result of lowering the normal force is a lower negative damping level. As a consequence, the region of coexistence of stable equilibria and stable limit cycles decreases, see figure 13(b).

5.2.2 Temperature Changes The experimental results corresponding to the nominal case are obtained when the temperature in the laboratory, where the set-up is placed, is between $25°\text{C}$ and $30°\text{C}$. The same results are collected when the temperature in the laboratory is between $17°\text{C}$ and $22°\text{C}$, for the same normal force applied at the brake ($20.5\,\text{N}$). The parameters of the obtained friction torque are estimated, the obtained model is validated and both the numerical and experimental bifurcation diagrams are constructed. The estimated friction torque at the lower part of the set-up is shown in figure 14(a). The related bifurcation diagrams are shown in figure 14(b) and the experimental results are once more predicted accurately by the model.

When the temperature is lower, the viscosity of the oil becomes higher. With such oil, the separation between the contacting surfaces (brake disc and the brake blocks in the experimental set-up) and the full fluid lubrication process occur for lower velocities. We have concluded that the position of the second Hopf bifurcation point is determined approximately by the angular velocity ω_l for which the friction force $T_{fl}(\omega_l)$ reaches its minimum (for $\omega_l > 0$), which corresponds to the point where full fluid lubrication appears (see figure 6). Consequently, the Hopf bifurcation point C', in figure 14(b), appears for lower input voltages than it does in the set-up when the temperature in the laboratory is higher.

Due to the fact that the viscous friction increases for lower temperatures the region of coexistence of stable equilibria and stable limit cycles decreases. Moreover, previously we have concluded that a higher viscous friction level causes the decrease of the amplitude of torsional vibrations and that the range of voltages in

which torsional vibrations can appear is smaller (compare figure 10 with figure 14).

6 Conclusions

In this paper, we investigate the way in which the occurrence and nature of friction-induced limit cycling in flexible mechanical systems (e.g. a drill-string system) depends on essential friction characteristics. This study is performed on the level of both model-based and experimental bifurcation analysis. The striking similarity of the model-based and experimental results confirms the quality of the model. The main conclusion, which is based on these combined results, is that a subtle interplay of negative damping characteristics at low velocities and viscous friction at higher velocities determines the occurrence and nature of the friction-induced limit cycling and the range of parameters for which these limit cycles sustain. Furthermore, we conclude that the the level of positive damping at very low velocities with respect to the negative damping level at slightly higher velocities determines whether torsional vibrations with and/or without stick-slip can occur. Moreover, results on both levels confirm that discontinuous bifurcations play a crucial role in the creation and destruction of these limit cycles.

The way in which such friction characteristics are influenced by physical conditions such as temperature and normal forces on the frictional contact is studied experimentally. An important observation is that the normal force in the frictional contact influences the friction force in a rather complex way and can induce a higher negative damping level (for higher normal forces), which in turn can give rise to limit cycles of higher amplitudes for a larger range of the constant input voltage.

It should be noted that the configuration of the experimental set-up (two masses, coupled by a flexibility, of which one is subject to friction and the other is driven by an actuator) can be recognized in many other mechanical systems, in which friction deteriorates the system performance by the induction of vibrations. In this context, one can think of printers, pick and place machines, industrial and domestic robots, simple earthquake models, accurate mirror positioning systems on satellites, drilling systems and many more. Finally, the insight gained by this work can very well be used to steer research on controller design for such systems aiming at the avoidance of friction-induced limit cycling.

References

Armstrong-Hélouvry, B., P. Dupont and C. Canudas de Wit (1994). A survey of models, analysis tools, and compensation methods for the control of machines with friction. *Automatica* **30**(7), 1083–1138.

Ascher, U. M., R. M. M. Mattheij and D. R. Russell (1995). *Numerical Solution of Boundary Value Problems for Ordinary Differential Equations*. SIAM. Philadelphia.

Brett, J. F. (1992). Genesis of torsional drillstring vibrations. *SPE Drilling Engineering* **7**(3), 168–174.

Brockley, C. A., R. Cameron and A. F. Potter (1967). Friction-induced vibrations. *ASME Journal of Lubrication Technology* **89**, 101–108.

Cunningham, R. A. (1968). Analysis of downhole measurements of drill string forces and motions. *ASME Journal of Engineering for Industry* **90**, 208–216.

Ibrahim, R. A. (1994a). Friction-induced vibration, chatter, squeal, and chaos: Mechanics of contact and friction. *Applied Mechanical Reviews: ASME* **47**(7), 209–226.

Ibrahim, R. A. (1994b). Friction-induced vibration, chatter, squeal, and chaos: Dynamics and modeling. *Applied Mechanical Reviews: ASME* **47**(7), 227–253.

Jansen, J. D. and L. van den Steen (1995). Active damping of self-excited torsional vibrations in oil well drillstrings. *Journal of Sound and Vibration* **179**(4), 647–668.

Krauter, A. I. (1981). Generation of squeal/chatter in water-lubricated elastomeric bearings. *ASME Journal of Lubrication Technology* **103**, 406–413.

Kreuzer, E. and O. Kust (1996). Analyse selbsterregter drehschwingugnen in torsionsstäben. *ZAMM - Journal of Applied Mathematics and Mechanics / Zeitschrift fuer Angewandte Mathematik und Mechanik* **76**(10), 547–557.

Leine, R. I. and H. Nijmeijer (2004). *Dynamics and Bifurcations of Non-smooth Mechanical Systems*. Springer. Berlin.

Leine, R. I., D. H. van Campen and W. J. G. Keultjes (2002). Stick-slip whirl interaction in drillstring dynamics. *ASME Journal of Vibrations and Acoustics* **124**, 209–220.

Mihajlović, N. (2005). Torsional and Lateral Vibrations in Flexible Rotor Systems with Friction. PhD thesis. Eindhoven University of Technology, The Netherlands.

Mihajlović, N., A. A. van Veggel, N. van de Wouw and H. Nijmeijer (2004). Friction-induced torsional vibrations in an experimental drill-string system. In: *Proceedings of the 23rd IASTED International conference on Modelling, Identification, and Control*. pp. 228–233.

Mihajlović, N., A. A. van Veggel, N. van de Wouw and H. Nijmeijer (2005*a*). Analysis of friction-induced limit cycling in an experimental drill-string set-up. *ASME Journal of Dynamic Systems, Measurements and Control*.

Mihajlović, N., N. van de Wouw, M. P. M. Hendriks and H. Nijmeijer (2005*b*). Friction-induced limit cycling in an experimental drill-string set-up for various friction situations. *Nonlinear Dynamics*. Submitted.

Parker, T. S. and L. O. Chua (1989). *Practical Numerical Algorithms for Chaotic Systems*. Springer-Verlag.

Popp, K., M. Rudolph, M. Kröger and M. Lindner (2002). Mechanisms to generate and to avoid friction induced vibrations. *VDI-Berichte 1736, VDI-Verlag Düsseldorf 2002* pp. 1–15.